The EMBO Journal vol.15 no.19 pp.5125–5134, 1996

Crystal structure of NH_3-dependent NAD^+ synthetase from *Bacillus subtilis*

Menico Rizzi[1,2], Claudio Nessi[1], Andrea Mattevi[1,3], Alessandro Coda[1,3], Martino Bolognesi[1,3,4] and Alessandro Galizzi[1,3]

[1]Department of Genetics and Microbiology 'A.Buzzati Traverso', University of Pavia, via Abbiategrasso 207, 27100 Pavia, [4]Department of Physics and IST–Advanced Biotechnology Centre, University of Genova, Largo R.Benzi, 16136 Genova and [3]CISMI, Centro Interuniversitario per lo Studio delle Macromolecole Informazionali, University of Pavia, 27100 Pavia, Italy

[2]Corresponding author

NAD^+ synthetase catalyzes the last step in the biosynthesis of nicotinamide adenine dinucleotide. The three-dimensional structure of NH_3-dependent NAD^+ synthetase from *Bacillus subtilis*, in its free form and in complex with ATP, has been solved by X-ray crystallography (at 2.6 and 2.0 Å resolution, respectively) using a combination of multiple isomorphous replacement and density modification techniques. The enzyme consists of a tight homodimer with α/β subunit topology. The catalytic site is located at the parallel β-sheet topological switch point, where one AMP molecule, one pyrophosphate and one Mg^{2+} ion are observed. Residue Ser46, part of the neighboring 'P-loop', is hydrogen bonded to the pyrophosphate group, and may play a role in promoting the adenylation of deamido-NAD^+ during the first step of the catalyzed reaction. The deamido-NAD^+ binding site, located at the subunit interface, is occupied by one ATP molecule, pointing towards the catalytic center. A conserved structural fingerprint of the catalytic site, comprising Ser46, is very reminiscent of a related protein region observed in glutamine-dependent GMP synthetase, supporting the hypothesis that NAD^+ synthetase belongs to the newly discovered family of 'N-type' ATP pyrophosphatases.

Keywords: amidotransferases/ATP pyrophophatases/ *Bacillus subtilis*/enzyme structure/NAD^+ synthetase

Introduction

Nicotinamide adenine dinucleotide (NAD^+) is a ubiquitous coenzyme involved in several biochemical processes such as oxidation–reduction reactions, DNA repair, DNA recombination and protein ADP ribosylations (Foster and Moat, 1980; Tritz, 1987). NAD^+ biosynthesis can be accomplished either through a *de novo* pathway or through a pyridine nucleotide salvage pathway (White, 1982). Both pathways have been characterized extensively in Gram-negative bacteria, while less is known for *Bacillus sp.* which are assumed to be similar to *Escherichia coli* and *Salmonella typhimurium*. The early part of the *de novo* pathway involves the enzymes L-aspartate oxidase, quinolinate synthetase and quinolinic acid phosphoribosyltransferase, which convert L-aspartic acid into nicotinic acid mononucleotide (NaMN). NaMN is then converted into nicotinic acid adenine dinucleotide (deamido-NAD^+), through the action of NaMN adenylyltransferase, and eventually into NAD^+ by means of NAD^+ synthetase. Once synthetized, NAD^+ can be recycled within one of the known salvage pathways (White, 1982).

The ubiquitous enzyme NAD^+ synthetase (EC 6.3.5.1) belongs to the amidotransferase family, an enzymatic family involved in a variety of biochemical processes, comprising synthesis of amino acids, purine and pyrimidine nucleotides, amino sugars, coenzymes and antibiotics (Zalkin, 1993; Smith, 1995). Amidotransferase enzymes are characterized by the presence of two separated domains which can belong to the same polypeptide chain or exist as independent subunits. A 'glutamine amide transfer' domain (GAT domain) is responsible for the ability to use glutamine as a nitrogen source, while the synthetase domain confers specificity and catalyzes the transfer of ammonia to the substrate (Zalkin, 1993). NAD^+ synthetase catalyzes the last step in NAD^+ biosynthesis, transforming deamido-NAD^+ into the final product NAD^+ by a two-step reaction, whereby the adenylation of deamido-NAD^+ is followed by addition of ammonia to the nicotinic acid carboxylate (Figure 1) (Spencer and Preiss, 1967).

The enzyme from *Bacillus subtilis*, which has been overexpressed in *E.coli*, consists of a functional homodimer, of 271 residues per chain, with a mol. wt of 60 480 Da (Nessi *et al.*, 1995). The enzyme has been shown to be involved in spore germination and outgrowth, through the isolation and characterization of temperature-sensitive mutants during spore germination (Albertini and Galizzi, 1975). Three additional mutants were isolated in a general screen for conditional lethal mutants of *B.subtilis* (Galizzi *et al.*, 1976; Caramori *et al.*, 1993). All mutants affected in NAD^+ synthetase activity were impaired in cellular functionality, thus indicating a major role for the enzyme in cellular metabolism. The mutant enzyme bearing the Gly156→Glu substitution is 200 times less active than the wild-type, producing a severe imbalance in NAD^+ metabolism (Nessi *et al.*, 1995). The enzyme isolated from *B.subtilis* is strictly ammonia dependent and is not able to utilize glutamine as a nitrogen source; the existence of an as yet uncharacterized second subunit bearing the GAT domain cannot, however, be ruled out.

On the basis of the above structural–functional information, and in the light of the recently determined crystal structure of GMP synthetase (Tesmer *et al.*, 1996), NAD^+ synthetase has been recognized as a member of a new family of 'N-type' ATP pyrophosphatases, which include asparagine synthetase and argininosuccinate synthetase. These enzymes are proposed to share a common

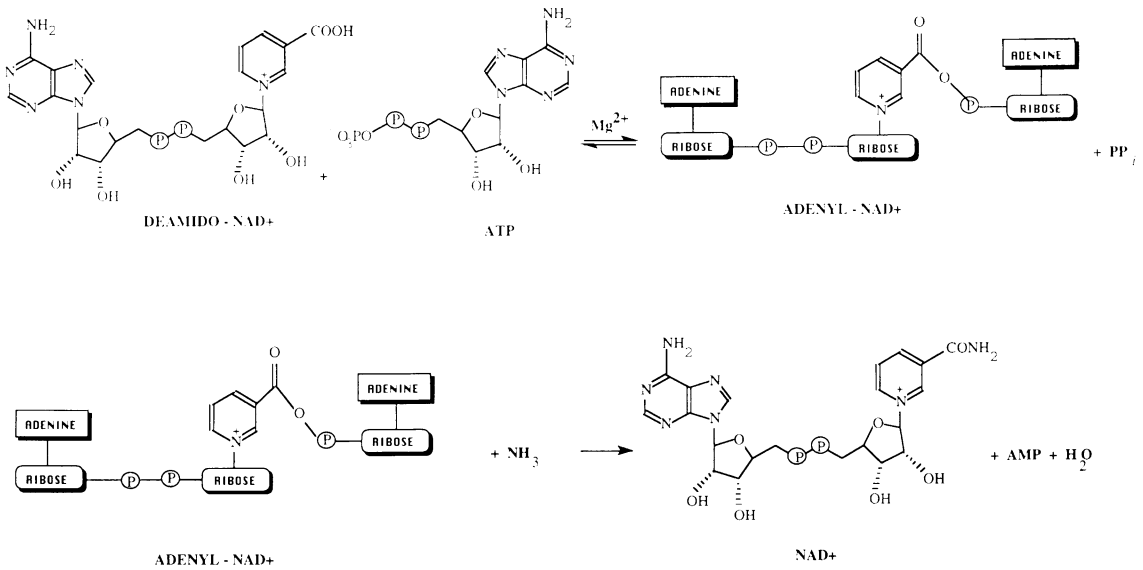

Fig. 1. A scheme of the two-step reaction catalyzed by NAD$^+$ synthetase.

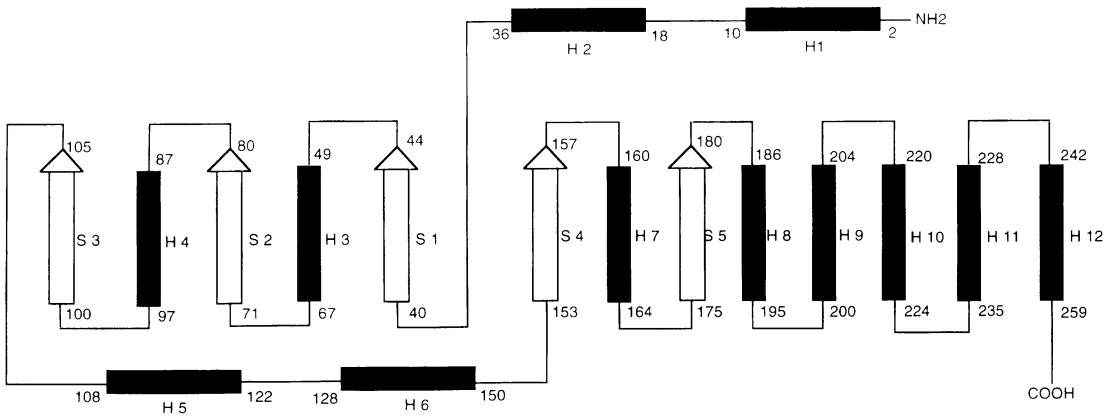

Fig. 2. Topology diagram of the NAD$^+$ synthetase subunit. White arrows and black cylinders represent β-strands and α-helices respectively.

mechanism of substrate adenylation, to promote subsequent amidation reactions, and are characterized by a conserved glycine-rich 'P-loop' sequence motif in the pyrophosphate (PP_i) binding site region. In this context, and considering that the enzyme is a potential target for the design of a new class of antibiotic compounds, we have determined the crystal structure of recombinant NAD$^+$ synthetase from *B.subtilis*, which is reported here in its free form (at 2.6 Å resolution) and in the ATP complex (at 2.0 Å resolution). The structure reveals a very compact homodimer with an extended subunit–subunit interface. The ATP and deamido-NAD$^+$ binding sites are located in deep clefts, on each subunit and at the dimer interface, respectively. Two polypeptide loops which are disordered in the free enzyme structure become fully structured upon ATP binding.

Results and discussion

Overall quality of the model

The structure of the free enzyme was solved by means of the multiple isomorphous replacement (MIR) method in conjunction with density modification techniques. The current model contains 490 residues and 116 solvent molecules with an *R*-factor of 0.189, and an *R*-free of 0.253, at 2.6 Å resolution; no interpretable electron density is present for the regions comprising residues 82–87 and 204–225.

The NAD$^+$ synthetase–ATP complex structure has been refined at 2.0 Å resolution to an *R*-factor of 0.174 and an *R*-free of 0.238. A final ($2F_o$–F_c) electron density map shows continuous density from residues 1 to 271 in both subunits. The refined model contains 542 residues, 228 solvent molecules, two pyrophosphate groups, two molecules of AMP and ATP and two Mg^{2+} ions. The stereochemistry of both refined models has been assessed with the program PROCHECK (Laskowski *et al.*, 1993); 95% of the residues are in the most favored regions of the Ramachandran plot and no outliers are present. Coordinates for both the free form and the ATP complex of NAD$^+$ synthetase have been deposited with the Brookhaven Protein Data Bank.

Overall structure

The polypeptide chain of each NAD$^+$ synthetase subunit is folded into five parallel β-strands, 12 α-helices and connecting loops; a schematic view of the secondary structure elements is reported in Figure 2. The protein achitecture consists of a single α/β domain, whose core

Fig. 3. Stereo ribbon representation of the subunit of NAD^+ synthetase, as produced by the program MOLSCRIPT (Kraulis, 1991). The parallel central β-sheet can be seen roughly edge-on with the ATP binding site, where AMP, PP_i and Mg^{2+} are shown as light blue ball-and-sticks and a blue sphere, respectively. The two loops, encompassing residues 82–87 and 205–224, undergoing structural reorganization upon ATP binding are shown as a green coil. The 'P-loop', connecting the S1 β-strand with helix H3 is shown as a violet coil.

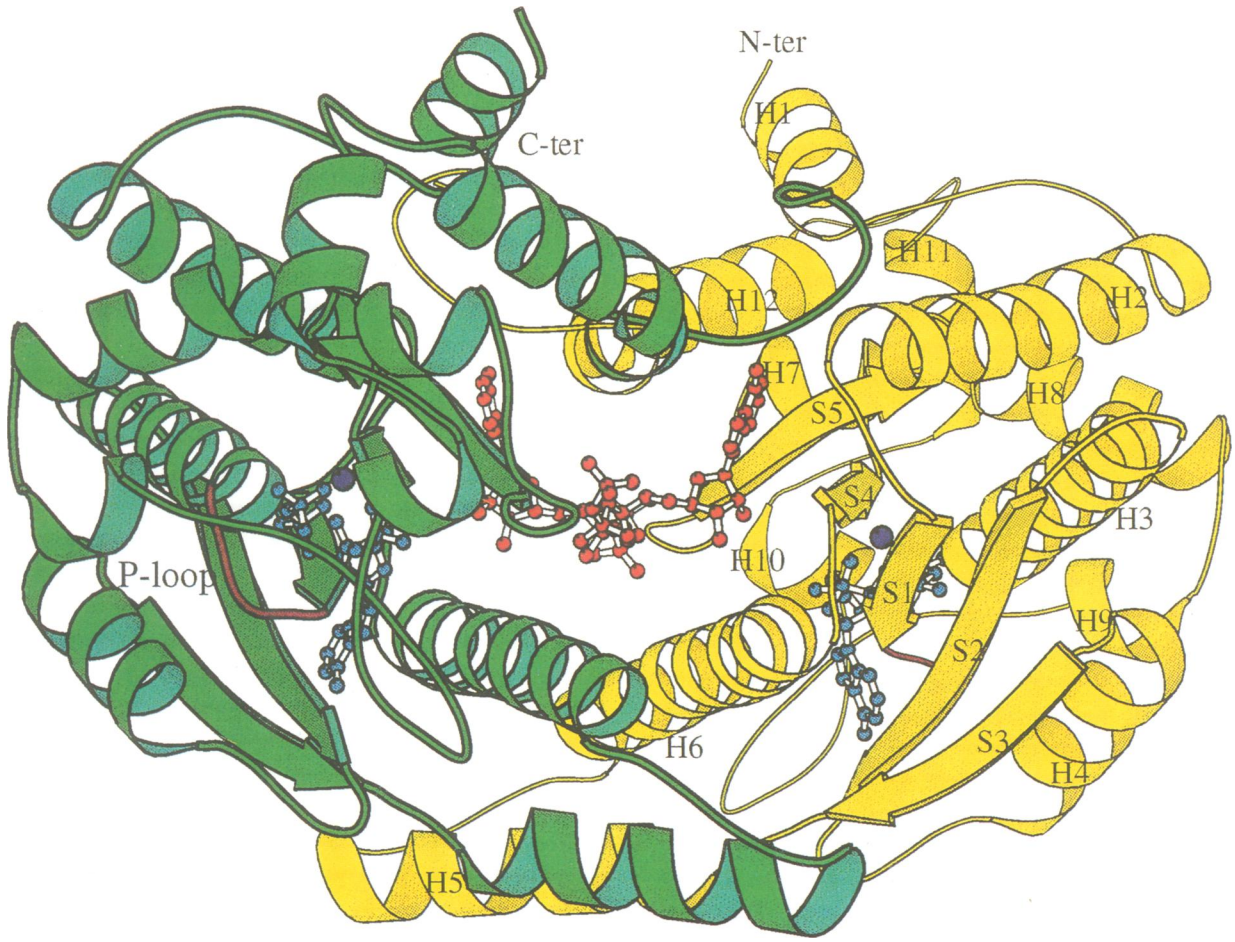

Fig. 4. Ribbon representation of the dimer of NAD^+ synthetase as produced by the program MOLSCRIPT (Kraulis, 1991) viewed perpendicular to the local dyad. The two subunits are colored in green and yellow. ATP (red), AMP (light blue) and PP_i (light blue) are shown as a ball-and-stick and Mg^{2+} as a blue sphere. The 'P-loop' is colored violet.

is a highly twisted five stranded parallel open β-sheet, flanked on both sides by α-helices (Figure 3). This topological organization closely resembles the well known six stranded dinucleotide binding domain (Rossmann *et al.*, 1975), except that in NAD^+ synthetase the sixth β-strand is substituted by a C-terminal extension of four α-helices.

The active NAD^+ synthetase homodimer is a 'heart shaped' molecule with approximate dimensions 43 Å × 38 Å × 65 Å (Figure 4). The two subunits are related by a local dyad. The dimer is very tight: 2678 $Å^2$ of the accessible surface area for each subunit (20% of their individual accessable surface areas) is buried upon dimer formation. This extended subunit interface, whose area falls in the upper limit of the range observed for oligomeric proteins (Janin *et al.*, 1988), may be related to the substantial stability reported for the dimeric enzyme (Nessi *et al.*, 1995).

The most striking feature in the subunit structure is represented by the extended C-terminal segment 260–271 and by a helix–loop motif (residues 108–127 comprising the H5 helix), which would protrude from a putative monomeric structure. These two regions resemble the arms of a clamp and anchor the two subunits to each other (Figure 4).

The dimer interface can be divided into two major regions which differ by the nature of the intermolecular contacts. The first region consists of an α-helical bundle, formed across the local 2-fold axis by helices H5 and H6 of each subunit. In forming the bundle, the H6 helices provided by the two subunits become buried deeply at the dimer interface. As a result, a number of hydrophobic intermolecular contacts are observed in their central regions, where MetA140 and IleA141 meet their equivalent residues in the facing subunit (contact distances of 3.5 and 3.6 Å, respectively). (Residues from the two subunits in NAD^+ synthetase are numbered A1–A271 and B1–B271, respectively.) Moreover, in the neighboring H5 helices, a stacking interaction is observed between the aromatic rings of PheA114 and PheB105, with a center–center distance of 3.5 Å.

The second contact region contributing to the dimer interface includes the C-terminal segment and residues 170–179. In this area, several polar interactions, involving both backbone and side chain atoms, are observed. In particular a salt bridge between AspA177 and LysB170 (2.7 Å), and three main chain hydrogen bonds, AspA177 N–ValB154 O (2.9 Å), AspA177 O–AlaB263 N (3.3 Å) and LeuA179 N–AlaB263 O (2.9 Å), are observed. Moreover, the rather extended conformation of the C-terminal residues allows the juxtaposition of residue TrpA270 from one subunit into an aromatic pocket (formed by residues TyrB32 and PheB28) on the surface of the other. The indole ring of the C-terminal TrpA270 (a residue conserved in the other NAD^+ synthetase amino acid sequences) is oriented edge-on with respect to the aromatic rings of TyrB32 and PheB28, with contact distances of 3.4 and 3.6 Å, respectively.

ATP binding site

The ATP binding site is located at the α/β open sheet topological switch point, firstly reported in dehydrogenases

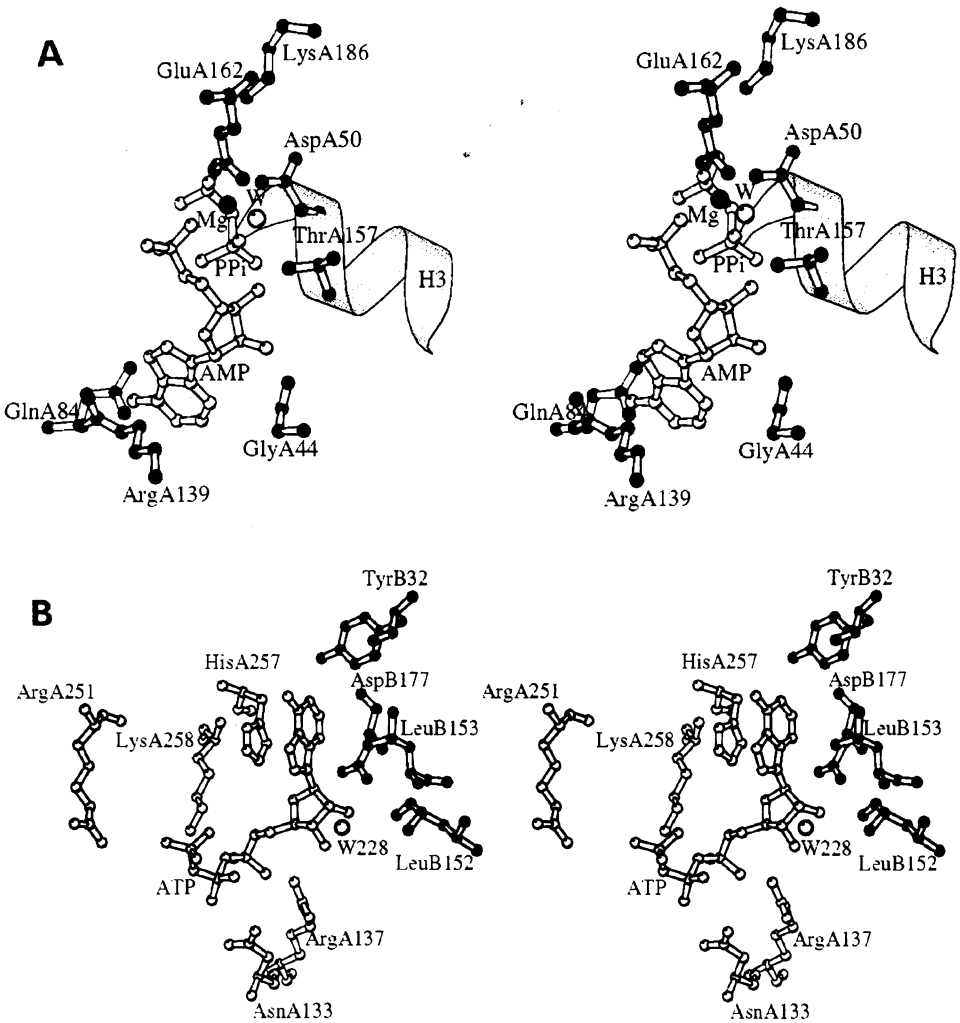

(Rossmann *et al.*, 1975), a deep cleft between the first (S1) and the fourth (S4) parallel β-strands (Figure 3). The enzyme soaked in ATP shows clear electron density in this pocket, compatible with AMP and PP_i. The 'P-loop' at the end of the S1 β-strand, peculiar to the nucleotide binding motif (Schulz, 1992), contains the fingerprint sequence Ser-Gly-Gly-X-Asp-Ser-Thr, which has been proposed to be characteristic of a new family of ATP pyrophosphatases (Tesmer *et al.*, 1996).

Several interactions stabilizing both the PP_i and the AMP moieties are observed, and account for the enzyme specificity with respect to ATP. All the protein residues involved in AMP and PP_i recognition are contributed by a single subunit, and no intermolecular interactions between the ATP binding pockets of the two subunits are present. The adenine ring of the bound AMP is stabilized primarily in its location by a hydrogen bond between its N6 atom and the OD1 atom of GlnA84 (2.8 Å), and by stacking with the guanidino group of ArgA139 (distance of 3.5 Å) (Figures 5A and 6). Moreover, the two hydroxyl groups of the ribose are hydrogen bonded to ThrA157 (2.8 Å) and to the carbonyl atom of GlyA44 (2.6 Å). Next to the AMP molecule, the PP_i anion is bound to the P-loop, making a total of five hydrogen bonds with protein residues (amongst them SerA46 and SerA51 OG atoms are at 2.7 and 2.6 Å, respectively, from the β-phosphate O atoms), whereas the γ-phosphate is salt bridged to LysA186 (2.7 Å). The βγ-bridge oxygen is centered at the N-terminus of the H3 helix, whose dipole (Hol *et al.*, 1978) participates in PP_i stabilization (Figures 5A and 6).

A strong peak in the F_o–F_c electron density map, bridging the AMP and PPi units, has been modeled as a Mg^{2+} ion, considering the crystallization medium composition and due to the ideal octahedral co-ordination observed, which is in keeping with the known co-ordination behavior of this cation in proteins as well as in co-ordinative complexes (Carugo *et al.*, 1993). The Mg^{2+} ligands are provided by the AspA50 OD1 atom (2.2 Å), the GluA162 OE1 atom (2.2 Å), by the β- and γ-phosphate O atoms, at 2.0 and 2.1 Å, respectively, and by the AMP α-phosphate O atom, at 2.2 Å. The coordinative sphere is completed by water molecule W216, at a distance of 2.0 Å (Figure 5A); the Mg^{2+} site is fully occupied and the cation displays a *B*-factor of 25 Å in both subunits.

Deamido-NAD+ binding site

The quaternary structure of NAD^+ synthetase defines two equivalent elongated clefts, each extending for ~20 Å at the subunit interface. The electron density observed in both clefts accounts for an intact ATP molecule, whose γ-phosphate group, however, displays *B*-factors >80 $Å^2$, this observation being compatible with the absence of a fixed location for the terminal phosphate. All the attempts made in order to obtain crystals of the enzyme with bound deamido-NAD^+ were unsuccessful because of severe crystal damage.

Inspection of the enzyme structure surrounding the bound ATP molecule (in each of the two equivalent clefts; Figures 5B and 6) shows that two residues contributed by the different subunits, HisA257 and LeuB153, clamp the adenosyl part of the bound nucleotide, fixing its orientation in the pocket such that two strong hydrogen bonds are

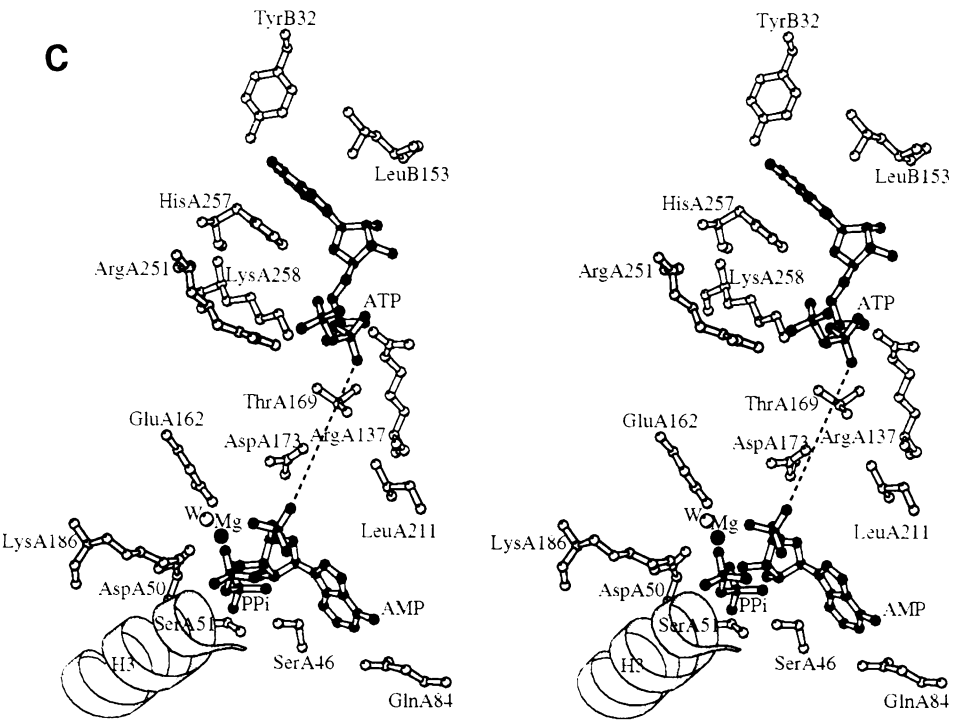

Fig. 5. (**A**) Stereo view of the ATP binding site. (**B**) Stereo view of the proposed deamido-NAD^+ binding site in the presence of one bound ATP molecule. A ball-and-stick representation has been adopted including residues of the B subunit (black), the A subunit (white) and the bound ATP (white). (**C**) Overall stereo view of the catalytic center of NAD^+ synthetase, including the ATP binding site (lower) and the deamido-NAD^+ binding site (upper); the dashed line connects the ATP and AMP closest atoms (9.8 Å) in the ATP-soaked crystals. (All generated using MOLSCRIPT; Kraulis, 1991.)

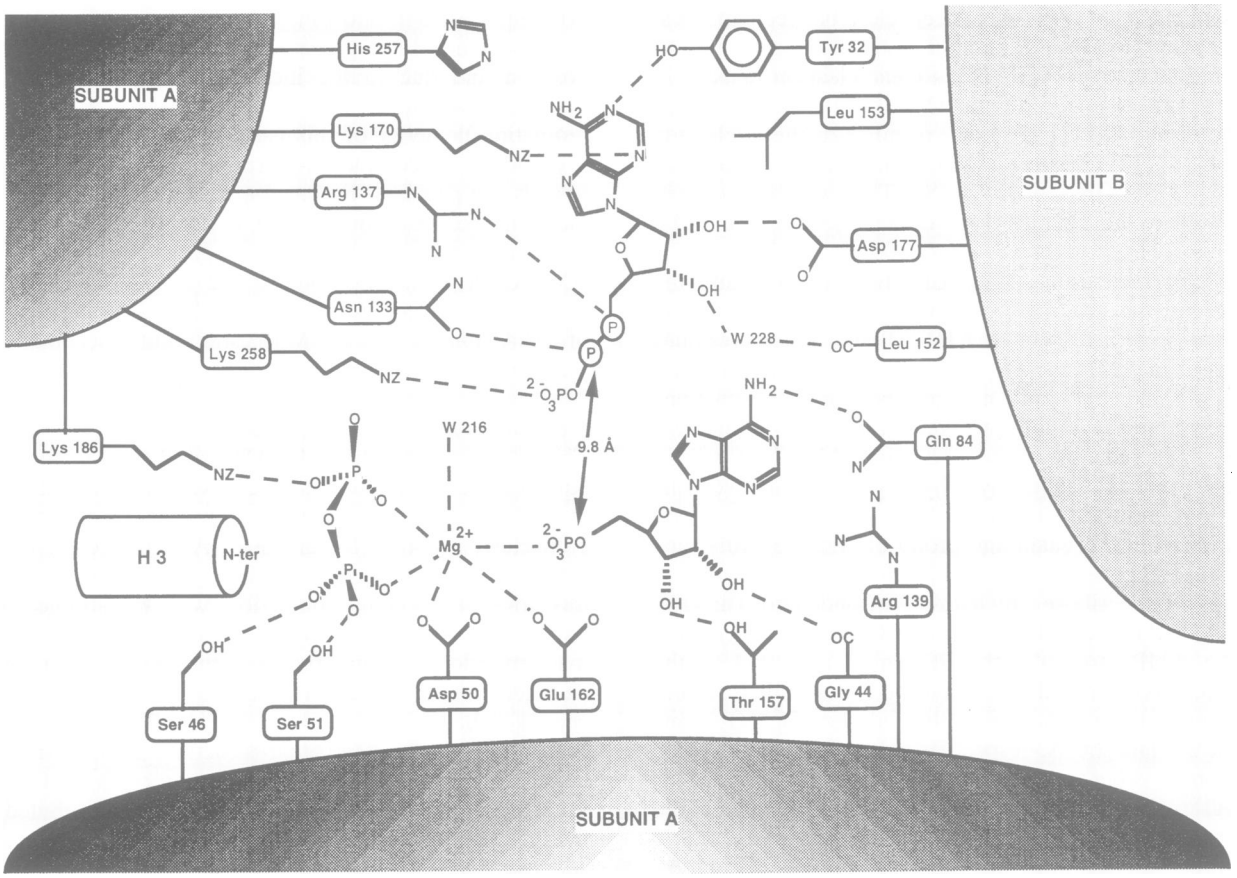

Fig. 6. A schematic representation of the interactions which have been recognized as involved in nucleotide recognition and binding in both the ATP and deamido-NAD^+ binding sites of NAD^+ synthetase. The dotted lines indicate interactions between connected atoms.

formed between the adenosyl N1 atom and the hydroxyl group of TyrB32 (2.6 Å), and between the adenosyl N3 atom and the NZ atom of LysA170 (3.2 Å) (Figures 5B and 6). The ribose moiety makes two hydrogen bonds, with AspB177 at 2.6 Å, and with W228 at 3.0 Å, which in turn is hydrogen bonded to the carbonyl group of LeuB152 (3.2 Å). It may be noticed that the presence of an aspartyl residue at the 177 sites should discriminate against the binding of $NADP^+$, which bears a phosphate group at the ribosyl 2′ position. At the opposite end of the ATP molecule, the phosphate groups are stabilized by residues provided by the other subunit. In fact, the α-phosphate is at 3.3 Å from the NH1 atom of ArgA137, the β-phosphate is 3.2 Å away from the OD1 atom of AsnA133 and the γ-terminal phosphate is at a distance of 3.3 Å from LysA258 (Figures 5B and 6).

Thus, considering the homodimeric structure of NAD^+ synthetase, the location of the two proposed deamido-NAD^+ binding sites at the subunit interface explains the requirement for a dimeric structure for the attainment of enzymatic activity. Such a proposal is supported further by the conservation of all residues identified above as being involved in nucleotide binding also in NAD^+ synthetase from *E.coli*, which is reported as a stable dimer (Willison and Tissot, 1994).

Mechanism of catalysis

Although the catalytic mechanism of NAD^+ synthetase has been analyzed so far only in general terms (Nessi *et al.*, 1995), the first structural evidence on the organization of the catalytic center, reported here, allows us to shed more light on the details of the reaction mechanism. As previously reported for the enzyme from *E.coli* (Spencer and Preiss, 1967), and confirmed by us (C.Nessi, unpublished results), the reaction proceeds through the adenylation of deamido-NAD^+ followed by the attachment of an NH_3 molecule onto the adenylated intermediate, resulting in the final product NAD^+ (Figure 1). As described above, we observe four major clefts in the dimeric enzyme, housing two ATP molecules at the subunit interface, and two AMP-PP_i-Mg^{2+} in deep clefts within each subunit. Orientation and nearest-neighbor considerations suggest that the two reactive species participating in the enzymatic reaction belong to different subunits, i.e. ATP from one subunit reacts with deamido-NAD^+ from the other (Figures 5C and 6). The distance between the nearest atoms of AMP and ATP observed in the complex structure is 9.8 Å. The empty space left, the structure of the bound nucleotide and the surrounding cavity allow us to model an entire molecule of deamido-NAD^+ into the site occupied by ATP in our crystals. Model building brings the second ribose moiety present in deamido-NAD^+ within hydrogen bonding distance of residues ThrA169 and AspA173. Moreover, the carboxylate of the nicotinic ring, in the modeled deamido-NAD^+, is located next to the α-phosphate of the bound AMP, correctly positioned to provide a nucleophilic attack on the α-phosphate of ATP during the first step of the catalytic cycle. A key role

in this respect could be played by the neighboring residue SerA46, which stabilizes the PP_i moiety through a hydrogen bond with its OG atom. This interaction could enhance the electrophilic character of the α-phosphate, facilitating its reactivity with deamido-NAD^+ in the first step of the catalyzed reaction. Similarly, the presence of the Mg^{2+} ion may be related not only to structural requirements, but also to its polarizing role (as a Lewis acid), favoring the nucleophilic attack on the α-phosphate and stabilizing the PP_i leaving group.

Several examples of enzymatic catalysis proceeding through adenylation of the substrate are known. Amongst them are tRNA synthetases, CoA ligases and luciferase (Delarue, 1995; McElroy *et al.*, 1967; Conti *et al.*, 1996). The exact roles of residues participating in catalysis and substrate binding have been studied extensively in tyrosyl-tRNA synthetase and glutamyl-tRNA synthetase, both structurally and by site-directed mutagenesis (Fersht, 1987; Perona *et al.*, 1993). In both enzymes, the activation of the substrate through adenylation is accounted for entirely by the binding energy, without any direct involvement of covalent or acid–base catalysis deriving from the enzyme functional groups (Fersht, 1987; Perona *et al.*, 1993). Such behavior seems unlikely in NAD^+ synthetase because both the sequence in the signature P-loop and the ATP binding mode are different from tRNA synthetases.

It has been reported previously that the Gly156→Glu mutation in NAD^+ synthetase results in an enzyme 200 times less active than the wild-type (Nessi *et al.*, 1995); the mutation strongly affects the K_m value for NH_3, leaving the K_m values for ATP and deamido-NAD^+ essentially unaltered. Gly156 is observed in the surrounding area of the ATP binding site at 6.7 Å from the nearest ATP atom. Modeling of the Glu156 side chain indicates that this residue is not compatible with direct interaction with ATP, in keeping with the unaltered K_m values. The replacement of a glycine with a negatively charged side chain could lead, on the other hand, to NH_3 sequestering, or create a steric hindrance to the incoming base.

A second mutation, resulting in a temperature-sensitive phenotype, has been identified in the gene coding for NAD^+ synthetase in *B.subtilis*, even if the mutated enzyme has not been purified and fully characterized (Caramori *et al.*, 1993). The reported mutation, His81→Tyr, occurs in the loop connecting the S2 β-strand with helix H4, on the protein surface, close to the ATP binding site. A tyrosyl residue in this position may form a hydrogen bond with AspA210, hampering access to the ATP binding site, and decreasing the enzyme's affinity for the nucleotide.

The comparison between the structures of free NAD^+ synthetase and its ATP adduct reveals major structural differences in two polypeptide loops neighboring the active site. The structure of the free enzyme was refined at 2.6 Å resolution, imposing strict non-crystallographic restraints, and did not reveal any electron density for the two regions encompassing residues 82–87 and 204–225, both in the surrounding area of the ATP binding site. We concluded that the two regions were disordered in the free enzyme, and were probably important in catalysis as they were located in the proximity of the catalytic site. Such a hypothesis was confirmed by the structure of the ATP adduct, refined at 2.0 Å resolution, which displays the 82–87 and 204–225 loops fully structured (Figure 3), suggesting their role in recognition/catalysis. Remarkable interactions between AMP-PP_i and residues of the two loops are indeed observed: GlnA84 is engaged in AMP stabilization (Figures 5A and 6), and two main chain hydrogen bonds, ThrA208 N–PPi O3G (3.2 Å) and ThrA208 O–AMP O3A (2.8 Å), are observed. Superposition of the structures of free and complexed NAD^+ synthetase (r.m.s. of 0.12 Å on all Cα atoms) reveals no other regions of significant conformational change.

The ATP pyrophosphatase family

NAD^+ synthetase has been proposed to be a member of a new ATP pyrophosphatase family on the basis of a conserved sequence fingerprint observed in GMP synthetase, argininosuccinate synthetase and asparagine synthetase (Tesmer *et al.* 1996). The three-dimensional structure determined in the present study confirms this proposal, revealing a common fold, partly shared by GMP and NAD^+ synthetases, as evidenced by the high score produced by the structural homology search program DALI (Holm and Sander, 1993). In fact, NAD^+ synthetase and the ATP pyrophosphatase domain of GMP synthetase, which share 20% sequence identity, can be superposed with an r.m.s. of 1.6 Å, for 116 Cα pairs (r.m.s. of 0.29 Å for Cα pairs of residues belonging to the 'P-loop'). The structurally homologous region includes the central β-sheet and the flanking α-helices, whereas no similarities are detectable for the remaining regions. The ATP binding site is remarkably similar in the two structures, with clearly conserved features such as residues SerA46 and SerA51, part of the 'P-loop', LysA186, salt bridged to the PP_i units, and the dipole of helix H3. Some notable substitutions, however, are also observed: residue ArgA139 in NAD^+ synthetase, which contacts the adenine ring, is replaced by Phe315 in GMP synthetase, which is oriented perpendicularly with respect to the adenine ring of AMP. Residue ThrA157, hydrogen bonded in NAD^+ synthetase to the ribose moiety of AMP, is occupied by Gly335 in GMP synthetase which thus cannot provide such a stabilizing interaction with the substrate. Remarkably, no hydrogen bonds between the adenine moiety of AMP and main chain atoms are observed in NAD^+ synthetase, as reported for GMP synthetase, where the only adenine–protein hydrogen bond is established between N6 and GlnA84 OD1 atoms. On the other hand, direct hydrogen bonding between the N6 atom of AMP and the protein backbone (Val260 O atom) is observed in GMP synthetase.

Materials and methods

Crystallization

The protein employed for crystallization was purified as previously described (Nessi *et al.*, 1995). Crystals of NAD^+ synthetase from *B.subtilis*, with average dimensions of 0.4×0.3×0.2 mm^3, were grown by dialysis from 22% v/v PEG 400, 0.05 M $MgCl_2$, 0.1 M sodium acetate, pH 5.2 at 28°C, at a protein concentration of 20 mg/ml, as reported elsewhere (Rizzi *et al.*, 1996). They belong to the monoclinic space group $P2_1$ with cells dimensions a = 53.0 Å, b = 87.1 Å, c = 60.2 Å and β = 111.1°; considering one NAD^+ synthetase dimer per asymmetric unit (60 480 Da), the calculated V_M is 2.15 $Å^3$/Da (Matthews, 1968), with a corresponding volume solvent content of 43%.

Crystals of the NAD^+ synthetase–ATP complex were obtained by co-crystallization using the hanging drop vapor diffusion technique. Drops containing 11% v/v PEG 400, 0.025 M $MgCl_2$, 0.005 M ATP, 0.003 M Triton X-100, 0.05 M sodium acetate, pH 5.2, with a protein concentration

Table I. Data collections statistics

Derivative	Resolution (Å)	Measurements	Independent reflections	Completeness (%)	R_{merge} (%)[a]	R_{iso} (%)[b]
Native	2.6	31 328	15 359	95.2	5.6	–
$LuCl_3$	3.0	53 831	10 381	98.6	11.5	14.6
$UO_2(NO_3)_2$	3.5	18 619	6309	95.6	10.1	18.6
ATP complex	2.0	177 041	33 464	94.0	6.4	30.0

[a]$R_{merge} = \Sigma|Ii-<Ii>|/\Sigma<Ii>$, where $<Ii>$ is the mean value of the ith intensity measurements.
[b]$R_{iso} = \Sigma||F_{ph}|-|F_p||/\Sigma|F_p|$, where F_{ph} and F_p are the derivative and native structure factors respectively.

of 20 mg/ml, were equilibrated against 22% PEG 400, 50 mM $MgCl_2$, 0.1 M sodium acetate, pH 5.2 at 20°C. The resulting crystals belong to space group $P2_1$ with cell dimensions a = 53.3 Å, b = 87.8 Å, c = 61.4 Å and β = 110.6°. Despite the fact that the free enzyme and the ATP complex crystals have similar cell parameters, evaluation of the diffracted intensities showed large variations between the two data sets (Table I).

Data collection and structure determination

For data collection and heavy atom screening, the free enzyme crystals were transferred in a stabilizing solution containing 26% v/v PEG 400, 0.05 M $MgCl_2$, 0.1 M sodium acetate, pH 5.2. All data sets used for MIR phasing were collected at room temperature on a Rigaku RAXIS II image plate system, using Cu Kα radiation. Diffracted intensities were evaluated and integrated using the program MOSFLM (A.Leslie), while the CCP4 suite was used for data reduction (CCP4, 1994). Table I gives a summary of the data collection statistics for the native protein as well as for the two heavy atom derivatives and for the ATP complex. The soaking time for the two derivatives was 8 h in the case of $LuCl_3$ and 48 h in the case of $UO_2(NO_3)_2$. The heavy atom concentrations were 1 and 0.5 mM respectively. The Lu^{3+} isomorphous difference Patterson map was solved using SHELX-90 (Sheldrick, 1991). The SIR phases thus obtained were used to locate the UO_2^{2+} binding sites by difference Fourier techniques. The heavy atom parameters were refined using MLPHARE (Otwinowski, 1991); phasing statistics are reported in Table II.

Although some secondary structure elements were clearly visible in the initial MIR electron density map, its overall quality did not allow chain tracing. However, the MIR phases were then improved substantially by means of 2-fold density averaging. The presence of a dimer in the asymmetric unit, suggested by the calculation of the V_M value, was confirmed by self-rotation function calculations, performed using the program AmoRe (Navaza, 1994). A strong peak (7.2σ over r.m.s.) located at κ = 180°, φ = 119.2°, ψ = 68.1° (Rossmann and Blow, 1962) clearly indicated the presence of a non-crystallographic 2-fold axis whose location in the asymmetric unit was determined by the program GLRF (Tong and Rossmann, 1990), used in the 'real space translation function' mode (option tfun = 2). The non-crystallographic operator was then refined with the subroutine CCMAX, part of the program DEMON (Vellieux *et al.*, 1995). A local correlation map calculation (Podjarny and Rees, 1991) was used for determination of the molecular envelope. The MIR phases were improved by simultaneous application of 2-fold density averaging, solvent flattening, histogram matching and map skeletonization with phase extension from 5.0 to 3.0 Å, as implemented in the program DM (CCP4, 1994). The resulting electron density map allowed us to trace ~90% of the protein model. The O package (Jones *et al.*, 1991) was used in the model-building stage, using the BATON option. A polypeptide chain was easily built; nevertheless, two major breaks were present in the electron density map, at residues 82–87 and 204–225.

Crystallographic refinement

Free enzyme. The crystallographic refinement was carried out at 2.6 Å resolution using X-PLOR (Brünger, 1992a) and the Engh–Huber stereochemical parameters (Engh and Huber, 1991). A random sample containing 5% of the total reflections (700 reflections) was excluded from the refinement and used for the calculation of the 'free' R-factor (Brünger, 1992b). Tight non-crystallographic symmetry restraints were maintained throughout all the different stages of refinement. The program O was used for manual rebuilding of the model (Jones *et al.*, 1991). The initial model (90% of the whole molecule) was subjected to 20 cycles of rigid body refinement in the 6.0–3.0 Å resolution range, lowering the R-factor and the R-free to 48 and 49%, respectively. Subsequently, 300 cycles of energy minimization, with tight non-crystallographic symmetry restraints, were performed, and a drop in the crystallographic R-factor to 32% (free R-factor 40%) was observed. At this stage of refinement, the electron density allowed sequence identification, and all the side chains were inserted in the model. An additional 300 cycles of refinement were carried out until convergence, giving an R-factor and a free R-factor of 26 and 36%, respectively. Final isotropic refinement of individual B-factors led to an R-factor of 18.9% and a free R-factor of 25.3%. Water molecules were added at positions with a density >3σ in the $2F_o-2F_c$ map, considering only peaks engaged in at least one hydrogen bond with a protein or a solvent atom.

The current model contains 505 amino acid residues and 116 water molecules. The polypeptide residues 82–87 and 204–225 are not visible in the electron density of both subunits. The average B-factors for the 3836 protein atoms and for the 116 ordered water molecules are 15.7 and 24.2 Å^2 (14.3 Å^2 for the main chain and 17.2 Å^2 for the side chains), respectively. The results of refinement are summarized in Table III.

ATP complex. The crystallographic refinement was performed in the 15.0–2.0 Å resolution range, using the TNT program package (Tronrud *et al.*, 1987), referring to the Engh–Huber stereochemical parameters

Table II. MIR phasing statistics

Derivative	Resolution (Å)	No. of sites	R_{cullis}[a]	Phasing power[b]	<FOM>[c]
$LuCl_3$	3.0	5	0.80	1.09	0.39
$UO_2(NO_3)_2$	3.5	2	0.79	1.53	

[a]$R_{cullis} = \Sigma||F_{PH} + F_P|-F_H|/\Sigma|F_{PH} + F_P|$ where F_P, F_{PH} and F_H are the observed protein, observed derivative and calculated heavy atom structure factors, with the sum over all centric reflections.
[b]Phasing power = $|F_H|/E$, where F_H is the calculated heavy atom structure factors and E is the residual lack of closure.
[c]$<FOM>$ (10.0–3.0 Å) = $\int P(\theta)\exp(i\theta)d\theta/\int P(\theta)d\theta$, where P is the probability distribution of the phase angle θ.

Table III. Refinement statistics

	Free enzyme	ATP complex
Resolution (Å)	6.0–2.6	15.0–2.0
No. of protein atoms	3836	4210
No. of solvent atoms	116	228
R-factor (%)[a]	18.9	17.4
R-free (%)[b]	25.3	23.8
ΔCα (Å)[c]	0.016	0.26
Root-mean-square deviations from ideality		
Bond lengths (Å)	0.020	0.015
Bond angles (°)	1.98	1.15
B-bonded atoms (Å^2)	3.2	5.3

[a]R-factor = $\Sigma|F_{obs}-F_{calc}|/\Sigma|F_{obs}|$.
[b]R-free = $\Sigma|F_{obs}-F_{calc}|/\Sigma|F_{obs}|$ (for the selected portion of all data).
[c]r.m.s. deviation for all Cα atoms after superposition of the two subunits.

(Engh and Huber, 1991), and excluding 5% (1668) randomly chosen reflections for the calculation of the 'free' *R*-factor (Brünger, 1992b). Neither NCS restraints nor structure factor sigma cutoff were applied. The initial *R*-factor, calculated with the refined coordinates of the free protein, was 40% at 2.0 Å resolution. This particularly high value was expected because of the substantial intensity differences observed between the apo-enzyme and the ATP complex data sets (Table II). Initial rigid-body refinement in the 15.0–3.0 Å resolution range resulted in a drop in the *R*-factor and *R*-free to 31 and 35%, respectively. Inspection of the $3F_o$–$2F_c$ and $2F_o$–$2F_c$ electron density maps allowed us unambiguously to trace the main chain for the two regions (82–87 and 204–225) unstructured in the apo-enzyme model. After 10 additional cycles of crystallographic restrained refinement, all the side chains for the two new regions were positioned in correct electron density. The entire model was then subjected to another series of refinement cycles until convergence was reached at an *R*-factor of 23.5% and an *R*-free of 31%, in the 15.0–2.0 Å resolution range. Solvent molecules were then added following the same criteria taken into account for the apo-enzyme. Inspection of the electron density maps at this stage showed (for each subunit) the presence of one intact ATP molecule bound at the subunit interface and of one AMP and PP_i in the extended ATP binding site. After fitting of the ATP, AMP and PP_i moieties, based on $3F_o$–$2F_c$ and $2F_o$–$2F_c$ electron density maps, five cycles of individual isotropic restrained *B*-factor and 10 cycles of positional restrained refinement were carried out. Convergence was reached at *R*-factor and *R*-free values of 17.4 and 23.8%, respectively, in the 15.0–2.0 Å resolution range. The final model consists of 4210 protein atoms (542 residues), 228 water molecules, two PP_i ions, two AMP molecules, two ATP molecules and two Mg^{2+} ions. The average *B*-factors for the protein atoms and for the solvent atoms are 27.4 and 37.1 Å^2, respectively. All the refined *B*-factors for the atoms of the two pyrophosphate and AMP units fall within the 15.0–32.0 Å^2 range. For the two ATP molecules, the same behavior is observed, with the exception of the terminal γ-phosphates, whose *B*-factors are >80.0 Å^2. Details of the refinement are reported in Table III.

Acknowledgements

The authors would like to thank all members of the Pavia protein crystallography group for their continuous interest in the project. M.A.Vanoni (University of Milano), S.Onesti (Imperial College, London) and J.L.Smith (Purdue University) are also acknowledged for helpful discussions. C.Nessi was supported by a grant from the Fond National Suisse pour la Recherche Scientifique. This research was supported in part by grants from Ministero dell'Università e della Ricerca Scientifica e Tecnologica (40%) and Progetto Finalizzato Ingegneria Proteica, CNR, Rome, and by Human Capital Mobility Program contract CT940690.

References

Albertini,A.M. and Galizzi,A. (1975) Mutant of *Bacillus subtlis* with a temperature-sensitive lesion in ribonucleic acid synthesis during germination. *J. Bacteriol.*, **124**, 14–25.

Brünger,A.T. (1992a) *A System for X-ray Crystallography NMR: XPLOR*. Version 3.1, Yale University Press, New Haven, CT.

Brünger,A.T. (1992b) The free *R* value: a novel statistical quantity for assessing the accuracy of crystal structures. *Nature*, **355**, 472–474.

Caramori,T., Calogero,S., Albertini,A. and Galizzi,A. (1993) Functional analysis of the *outB* gene of *Bacillus subtilis*. *J. Gen. Microbiol.*, **139**, 31–37.

Carugo,O., Djinovic,K. and Rizzi,M. (1993) Comparison of the co-ordinative behaviour of calcium (II) and magnesium (II) from crystallographic data. *J. Chem. Soc. Dalton Trans.*, 2127–2135.

Collaborative Computational Project Number 4 (1994) The CCP4 suite: programs for protein crystallography. *Acta Crystallogr.*, **D50**, 760–767.

Conti,E., Franks,N.P. and Brick,P. (1996) Crystal structure of firefly luciferase throws light on a superfamily of adenylate-forming enzymes. *Structure*, **4**, 287–298.

Delarue,M. (1995) Aminoacyl-tRNA synthetase. *Curr. Opin. Struct. Biol.*, **5**, 48–55.

Engh,R.A. and Huber,R. (1991) Accurate bond angles and parameters for X-ray protein structure refinement. *Acta Crystallogr.*, **A45**, 392–400.

Fersth,A.R. (1987) Dissection of the structure and activity of the tyrosyl-tRNA synthetase by site-directed mutagenesis. *Biochemistry*, **26**, 8031–8037.

Foster,J.W. and Moat,A.G. (1980) Nicotinamide adenine dinucleotide biosynthesis and pyridine nucleotide cycle metabolism in microbial systems. *Microbiol. Rev.*, **44**, 83–105.

Galizzi,A., Siccardi,A.G., Mazza,G., Canosi,U. and Polsinelli,M. (1976) A recombination test to classify mutants of *Bacillus subtilis* of identical phenotype. *Genet. Res.*, **27**, 47–58.

Hol,W.G.J., van Duijnen,P.T. and Berendsen,H.J.C. (1978) The α-helix dipole and the properties of proteins. *Nature*, **273**, 443–446.

Holm,L. and Sander,C. (1993) Protein structure comparison by alignment of distance matrices. *J. Mol. Biol.*, **233**, 123–138.

Janin,J., Miller,S. and Chothia,C. (1988) Surface, subunit interfaces and interior of oligomeric proteins. *J. Mol. Biol.*, **204**, 155–164.

Jones,T.A., Zou,J.Y., Cowan,S.W. and Kjeldgaard,M. (1991) Improved methods for building models in electron density maps and the location of errors in these models. *Acta Crystallogr.*, **A47**, 110–119.

Kraulis,P.J. (1991) MOLSCRIPT: a program to produce both detailed and schematic plots of protein structures. *J. Appl. Crystallogr.*, **24**, 946–950.

Laskowski,R.A., MacArthur,M.W., Moss,D.S. and Thornton,J.M. (1993) PROCHECK: a program to check the stereochemistry of protein structures. *J. Appl. Crystallogr.*, **26**, 283–291.

Matthews,B.W. (1968) Solvent content of protein crystals. *J. Mol. Biol.*, **33**, 491–497.

McElroy,W.D., DeLuca,M. and Travis,J. (1967) Molecular uniformity in biological catalyses. The enzymes concerned with firefly luciferin, amino acid, and fatty acid utilization are compared. *Science*, **157**, 150–160.

Navaza,J. (1994) AMoRe: an automated procedure for molecular replacement. *Acta Crystallogr.*, **A50**, 157–163.

Nessi,C., Albertini,A.M., Speranza,M.L. and Galizzi,A. (1995) The *outB* gene of *Bacillus subtlis* codes for NAD synthetase. *J. Biol. Chem.*, **270**, 6181–6185.

Otwinowski,Z. (1991) Maximum likelihood refinement of heavy atom parameters. In Wolf,W., Evans,P.R. and Leslie,A.G.W. (eds), *Isomorphous Replacement and Anomalous Scattering. Proceedings of the CCP4 Study Weekend 25–26 January 1991*. SERC, Daresbury Laboratory, Warrington, UK, pp. 80–86.

Perona,J.J., Rould,M. and Steitz,T.A. (1993) Structural basis for transfer RNA aminoacylation by *Escherichia coli* glutamyl-tRNA synthetase. *Biochemistry*, **32**, 8758–8771.

Podjarny,A.D. and Rees,B. (1991) Density modification: theory and practice. In Moras,D., Podjarny,A.D. and Thierry,J.C. (eds), *Crystallographic Computing 5: From Chemistry to Biology*. Oxford University Press, Oxford, pp. 361–372.

Rizzi,M., Nessi,C., Bolognesi,M., Coda,A. and Galizzi,A. (1996) Crystallization of NAD$^-$ synthetase from *Bacillus subtilis*. *Proteins: Structure, Funct. Genet.*, in press.

Rossmann,M.G. and Blow,D.M. (1962) The detections of sub-units within the crystallographic asymmetric unit. *Acta Crystallogr.*, **15**, 24–31.

Rossmann,M.G., Liljas,A., Branden,C.I. and Banaszak,L.J. (1975) In Boyer,P.D. (ed.), *The Enzymes*. Academic Press, New York, pp. 61–102.

Schulz,G.E. (1992) Binding of nucleotides by proteins. *Curr. Opin. Struct. Biol.*, **2**, 61–67.

Sheldrick,G.M. (1991) Heavy atom location using SHELXS-90. In *Isomorphous Replacement and Anomalous Scattering. Proceedings of the CCP4 Study Weekend 25–26 January 1991*. SERC, Daresbury Laboratory, Warrington, UK, pp. 23–38.

Smith,L.J. (1995) Enzymes of nucleotide synthesis. *Curr. Opin. Struct. Biol.*, **5**, 752–757.

Spencer,R.L. and Preiss,J. (1967) Biosynthesis of diphosphopyridine nucleotide: the purification and the properties of diphosphopyridine nucleotide synthetase from *Escherichia coli*. *J. Biol. Chem.*, **242**, 385–392.

Tesmer,J.G., Klem,T.J., Deras,M.L., Davisson,V.J. and Smith,J. (1996) The crystal structure of GMP synthetase reveals a novel catalytic triad and is a structural paradigm for two enzyme families. *Nature Struct. Biol.*, **3**, 74–86.

Tong,L. and Rossmann,M.G. (1990) The locked rotation function. *Acta Crystallogr.*, **A46**, 783–792.

Tritz,G.J. (1987) NAD biosynthesis and recycling. In Neidhardt,F.C., Ingraham,J.L., Brooks Low,K., Magasanik,B., Schaechter,M. and Umbarger,H.E. (eds), *Escherichia coli and Salmonella typhimurium Cellular and Molecular Biology*. American Society for Microbiology, Washington DC, Vol. 1, pp. 557–563.

Tronrud,D.E., Ten Eyck,L.F. and Matthews,B.W. (1987) An efficient general-purpose least-squares refinement program for macromolecular structures. *Acta Crystallogr.*, **A43**, 489–501.

Vellieux,F.M.D.V., Hunt,J.F., Roy,S. and Read,R.J. (1995) DEMON/ANGEL: a suite of programs to carry out density modification. *J. Appl. Crystallogr.*, **28**, 347–351.

White,H.B. (1982) Biosynthesis of salvage pathaways of pyridine nucleotide coenzymes. In Everse,J., Anderson,B.M. and You,K.S. (eds), *Pyridine Nucleotide Coenzyme*. Academic Press Inc., New York, pp. 1–17.

Willison,J.C. and Tissot,G. (1994) The *Escherichia coli efg* gene and the *Rhodobacter capsulatus adgA* gene code for NH_3-dependent NAD^+ synthetase. *J. Bacteriol.*, **176**, 3400–3402.

Zalkin,H. (1993) The amidotransferases. *Adv. Enzymol. Relat. Areas Mol. Biol.*, **66**, 203–309.

Received on April 24, 1996; revised on June 11, 1996